SUPPORTING INFORMATION

Controlling the morphology of model conjugated thiophene oligomers through alkyl side chain length, placement and interactions

Hilary S. Marsh†, Eric Jankowski†, and Arthi Jayaraman*

Department of Chemical and Biological Engineering, UCB 596, University of Colorado Boulder CO 80309

* corresponding author (arthi.jayaraman@colorado.edu)

† Equal Contributions

This supporting material contains the following sections:

Section I: Model and Simulation

Section II: Criteria for Choosing Snapshots for Data Analysis

Section III: Additional Results

LIST OF FIGURES AND TABLES

Section I: Model and Simulation

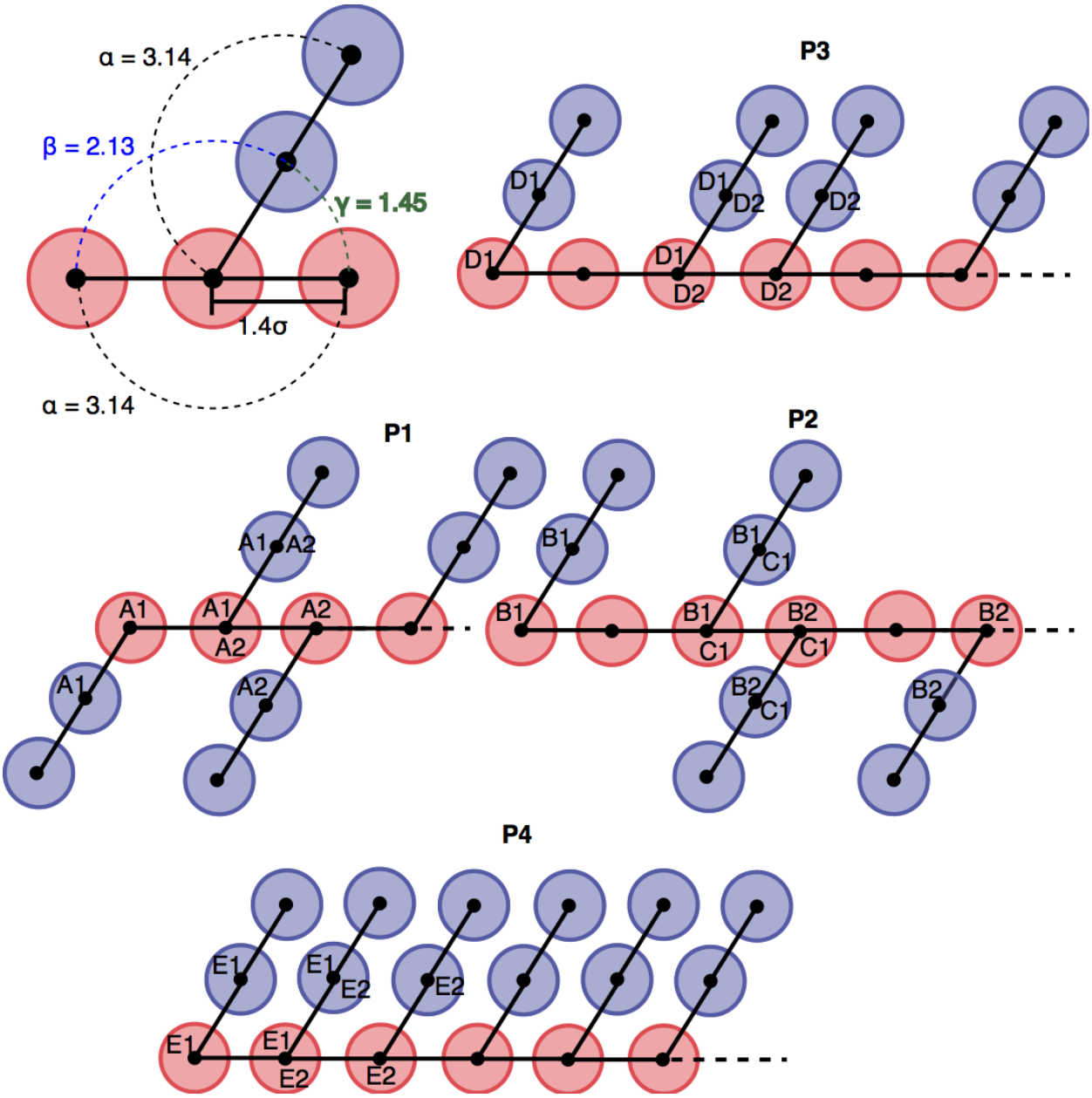

Figure S.0: Connectivity of coarse-grained beads and the associated angle and dihedral constraints for oligomers P1, P2, P3, and P4. The four oligomers differ in the number of side chains and the dihedral angle constraints imposed to maintain their respective architectures. Five different dihedral angle types are denoted by the letters A-E. Examples of four beads comprising a dihedral angle constraint are indicated with a letter and number (e.g., A1 beads are all part of a type A dihedral angle constraint, and A2 beads are part of a different type A dihedral angle constraint). Dashed lines indicate where additional monomers are added to the shown schematics to complete the 15-bead oligomers.

Of the four oligomer architectures used in this work, P1, P2, and P3 are identical to those used in Jankowski, Marsh, and Jayaraman, *Macromolecules 46, 14 (2013),* and are shown In Figure S.0. Oligomer P4 is similar to oligomer P3 in that each side chain extends along the same side of the backbone, but P4 has side chains extending from each backbone bead. Harmonic potentials model bond stretching constraints ($U_{bond} = k_{bond}(l - l_0)^2$), angle bending constraints ($U_{angle} = k_{angle}(\theta - \theta_0)^2$), and dihedral angle twisting constraints ($U_{di} = k_{di}(\phi - \phi_0)^2$), as in Jankowski, Marsh, and Jayaraman, *Macromolecules 46, 14 (2013)*, with the same spring constants: $k_{bond} = 50\ \varepsilon/\sigma^2$ for all bonded pairs, $k_{angle} = 6\ \varepsilon/\text{radian}^2$ for three body angle potentials with equilibrium angles $\beta = 2.13$ and $\gamma = 1.45$, and is $30\ \varepsilon/\text{radian}^2$ for angle $\alpha = 3.14$. The side chains of P1 are constrained only with dihedral angle A, which has equilibrium angle 3.14 (e.g., the four A1's or the four A2's in Figure S.0.) and spring constant $10\ \varepsilon/\text{radian}^2$. The topology of P2 is maintained by dihedral angles B (equilibrium angle 0, spring constant $50\ \varepsilon/\text{radian}^2$) and C (equilibrium angle 3.14, spring constant $50\ \varepsilon/\text{radian}^2$). The topology of P3 is maintained by dihedral angle D (equilibrium angle 0, spring constant $10\ \varepsilon/\text{radian}^2$). The topology of P4 is maintained by dihedral angle E (equilibrium angle 0, spring constant $10\ \varepsilon/\text{radian}^2$).

Section II: Criteria for Choosing Snapshots for Data Analysis

Three criteria must be met for snapshots from a simulation trajectory to be used as statistically independent, equilibrated snapshots for data analysis. These are as follows:

The first criterion, that at least 20 **snapshots from the end of a trajectory are statistically independent**, is determined by using the autocorrelation time of the potential energy time series as a proxy for the autocorrelation time of structure. The potential energy autocorrelation time *a* is measured by identifying the first zero of

$$C(dt) = \frac{\langle (PE(t) - A)(PE(t+dt) - A) \rangle}{\sigma^2}$$

where *PE(t)* is the instantaneous potential energy at time *t*, with average *A* and variance σ^2 (not to be confused with particle diameter σ) over a subset of full potential energy time series. The first criterion is satisfied if there exists a subset of the potential energy time series with range $(t_{max} - t_{min}) > 20a$.

The second criterion, that the **structure observed is not dependent upon the shape of the simulation box**, is satisfied through the use of secondary simulations in which the periodic box axes are allowed to vary independently and as determined by the diagonal components of the pressure tensor. These "orthorhombic" simulations either show that the structure from the simulations with cubic boxes are stable under anisotropic box deformations, or allow the periodic spacing of features to relax slightly (typically a few 0.1 σ). The autocorrelation time criterion mentioned above is imposed on the orthorhombic simulation trajectories.

The third and final criterion that must be met is that no periodic box axis is short enough (22.1 σ) to allow for an oligomer to interact with itself through a periodic boundary. For three systems,

P1b T* = 1.5, P4b T* = 1.5 and P4b T* = 1.75, we observed one box axis becoming shorter than 22.1 σ before 20 independent configurations were achieved in the orthorhombic runs. For these systems, we performed additional simulations for each system, using non-cubic boxes from the orthorhombic runs as initial conditions in NPT simulations with isotropic pressure integration.

Section III: Additional Results

Table S.1: Exposed backbone area calculated using the solvent available surface area method averaged over 20 snapshots for oligomers P1, P2, P3, and P4 at T* = 1.5. The average exposed backbone areas, A_E, plotted in Figure 3 in the main manuscript are the average of the exposed backbone areas of the four side chain types, *a*, *b*, *c*, and *d*, for each oligomer P1, P2, P3, and P4 at T* = 1.5 shown in this table.

	Backbone Area [σ^2]	+/-
P1a	151.4	44.3
P1b	132.1	60.1
P1c	148.9	44.7
P1d	127.4	32.8
P2a	236.3	48.9
P2b	239.0	42.2
P2c	259.1	52.0
P2d	225.1	58.0
P3a	286.9	50.4
P3b	277.0	51.1
P3c	265.9	56.0
P3d	277.5	50.1
P4a	257.7	47.7
P4b	237.0	55.4
P4c	281.9	52.0
P4d	239.0	59.7

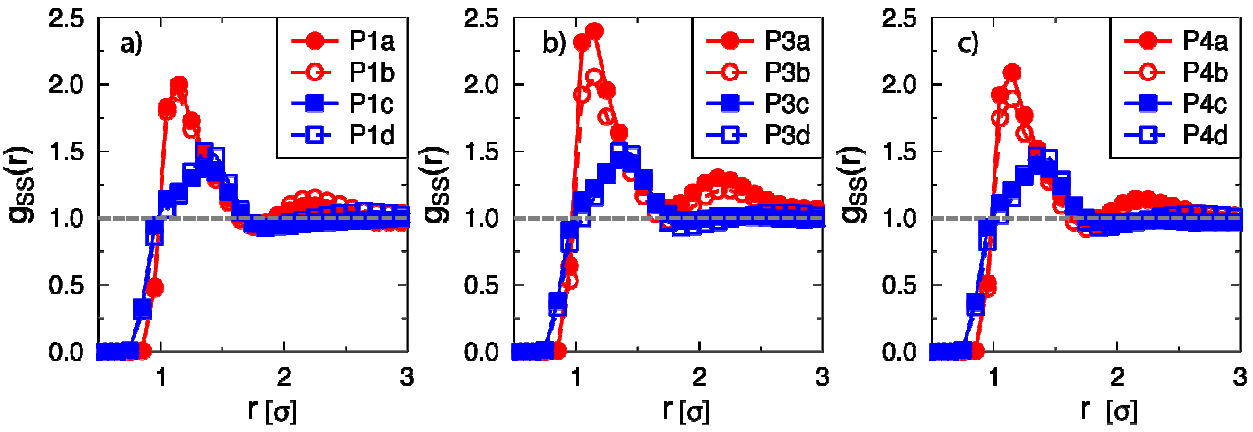

Figure S.1: Side chain – side chain radial distribution function, $g_{SS}(r)$, as a function of reduced distance, r, for a) P1, b) P3, and c) P4 for side chain types *a*, *b*, *c*, and *d*, at T* = 1.5. The plot of $g_{SS}(r)$ for P2 is found in the main manuscript, Figure 3. As for oligomer P2, the $g_{SS}(r)$ plots for oligomers P1, P3, and P4 show that at a given temperature, moderately attractive side chains are highly aggregated at the separation distance at the Lennard-Jones potential minimum (r~=1.15 σ), and weakly attractive side chains show relatively less coordination at peak distance r~=1.4 σ. The peak distance of r ~= 1.4 σ matches the equilibrium bond length between side chain beads of 1.4 σ, demonstrating that there is negligible side chain aggregation due to non-bonded attractive interactions for all four oligomers at weak side chain – side chain attraction.

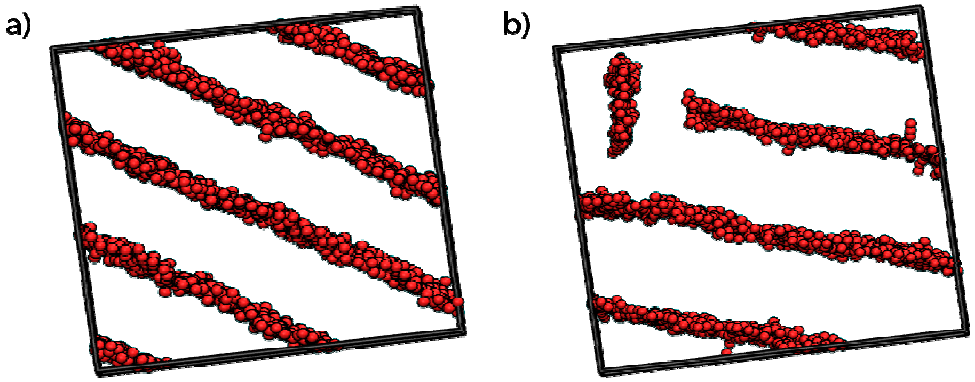

Figure S.2: a) Snapshot of equilibrated P1b (ε_{SS} = 1.0) lamellae T* = 1.5. b) Snapshot of simulation at T* = 1.25 with the starting configuration shown in part (a) after transformation to P1d (setting ε_{SS} = 0.1) and equilibration. Lamellae transform into perforated lamellae with the introduction of weak side chain – side chain interaction potentials (ε_{SS} = 0.1) suggesting that the perforated lamellar phase is stable for P1d at T* = 1.25.

Table S.2: Widths of backbone lamellae for systems of oligomers P1 and P2 at temperatures $T^* \leq T^*_{ODT}$. Lamellar widths are not reported at temperatures where the oligomer is disordered, denoted by, D, or at temperatures where simulations were not performed, denoted by "--". The widths of the backbone lamellae are greater for P2 than for P1. Spherical backbone beads in our model are able to hexagonally pack and the decreased side chain density for P2 compared to P1 promotes this packing and increases lamellar thickness for P2 compared to P1.

	P1		**P2**	
	Width [σ]	**+/-**	**Width [σ]**	**+/-**
a T* = 1.5	0.68	0.06	0.90	0.04
a T* = 1.75	0.85	0.12	0.89	0.05
b T* = 1.5	0.53	0.19	0.96	0.02
b T* = 1.75	0.63	0.09	0.91	0.05
b T* = 2.0	D	D	0.90	0.02
c T* = 1.25	0.52	0.09	--	--
c T* = 1.5	D	D	0.81	0.05
c T* = 1.75	D	D	0.87	0.02
d T* = 1.25	0.62	0.18	--	--
d T* = 1.5	D	D	0.97	0.06
d T* = 1.75	D	D	0.85	0.10

Supporting Movie SM1: To determine whether the *–anti* orientation of P2b side chains inhibits the formation of the cylinders that form for P3b with *–syn* oriented side chains, we continue the equilibrated simulation of P2b at T* = 2.0 with the dihedral angle bond constants set to 0. Within 5e7 time steps, the P2b lamellae transform into cylinders with oligomer side chains in the *-syn* orientation. Thus, oligomer architectures with side chains in the *–anti* orientation prevent the formation of the energetically favorable cylindrical phase.

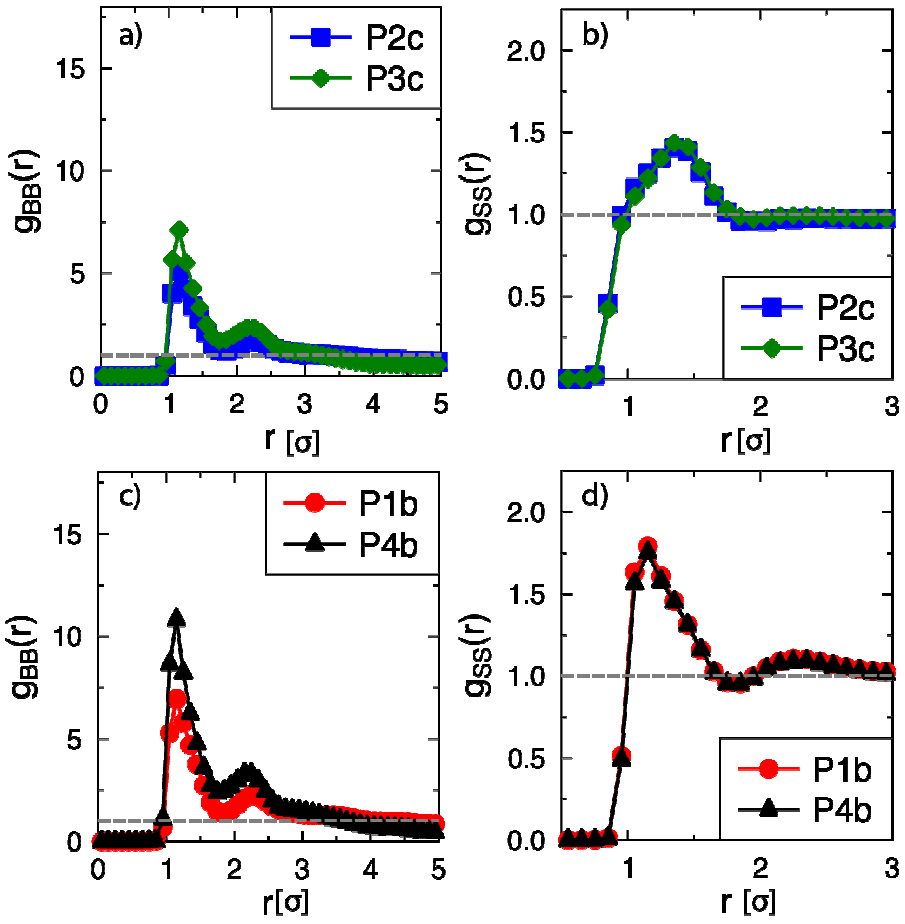

Figure S.3: a) Backbone- backbone radial distribution function, $g_{BB}(r)$, and b) side chain – side chain radial distribution function, $g_{SS}(r)$, as a function reduced distance, r, for oligomers P2c and P3c at T* = 1.75. c) $g_{BB}(r)$, and d) $g_{SS}(r)$ for oligomers P1b and P4b at T* = 1.75. P1 and P2 have side chains in the *–anti* orientation and form lamellae at T* = 1.75 while P3 and P4 have side chains in the *–syn* orientation and form cylinders at T* = 1.75. P2 and P3 have the same density of side chains and P1 and P4 have the same density of side chains so these systems with equal side chain density are compared to isolate the effect of side chain orientation on morphology. In both cases, the cylindrical phase (P3c or P4b) is energetically favorable and allows for more backbone-backbone contacts than does the lamellar phase (P2c or P1b, respectively) (Figure S.2a and c). $g_{SS}(r)$ does not change significantly between P2c and P3c, or between P1b and P4b (Figure S.2b and d, respectively). Thus, side chain orientation and equilibrium morphology do not impact the number of side chain – side chain contacts. These trends match those for the comparison of P2b and P3b shown in the main manuscript.

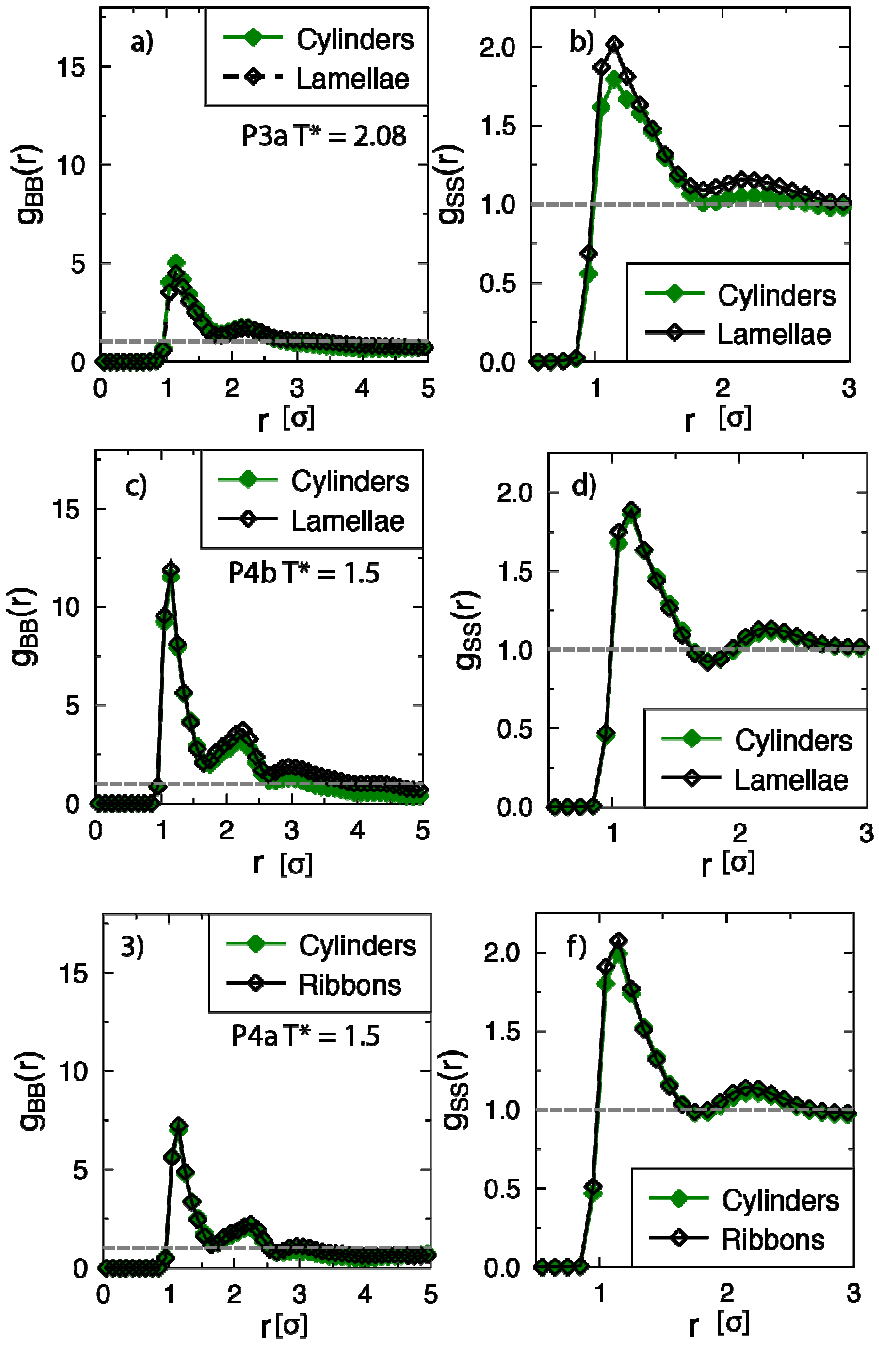

Figure S.4: a) Backbone - backbone radial distribution function, $g_{BB}(r)$, and b) side chain – side chain radial distribution function, $g_{SS}(r)$, as a function reduced distance, r, for oligomer P3a at T* = 2.08 before the and after the phase transition from cylinders to lamellae. c) $g_{BB}(r)$, and d) $g_{SS}(r)$ for oligomer P4b T* = 1.5 before the and after the phase transition from cylinders to lamellae. e) $g_{BB}(r)$ and f) $g_{SS}(r)$, for oligomer P4a T* = 1.5 before the and after the phase transition from cylinders to ribbons. The $g_{BB}(r)$ and $g_{SS}(r)$ plots show that there is little change in the number of backbone – backbone and side chain – side chain contacts at the transition temperature for P4b and P4a and this trend is consistent with the data shown for P3b in the main manuscript. P3a

cylinders have slightly more backbone – backbone contacts and slightly fewer side chain contacts than do P3a lamellae after the transition.

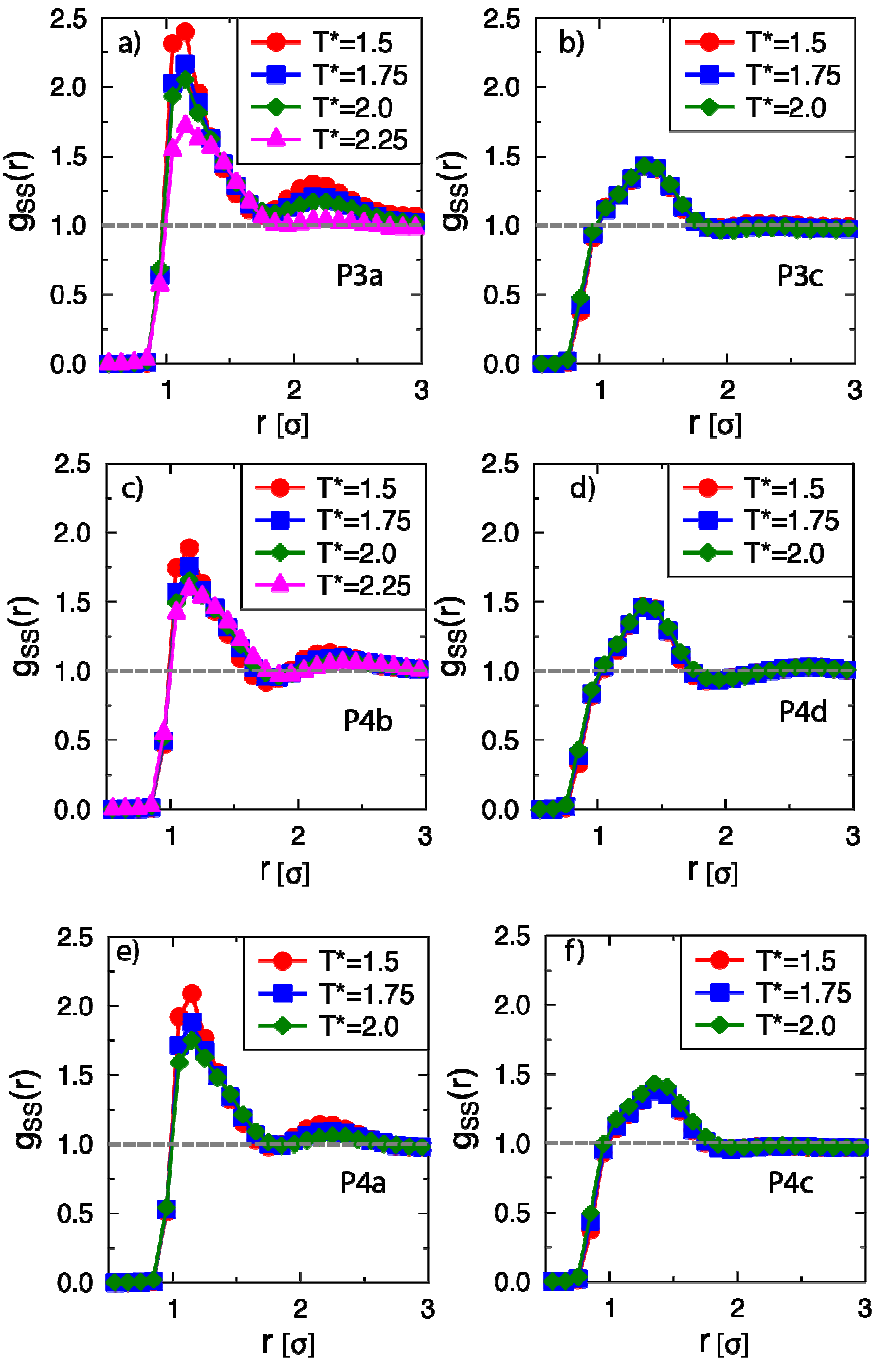

Figure S.5: a) Side chain – side chain radial distribution function, $g_{SS}(r)$, as a function reduced distance, r, for oligomer P3a at T* = 1.5, 1.75, 2.0 and 2.25. b) $g_{SS}(r)$ for oligomer P3c at T* = 1.5, 1.75 and 2.0. c) $g_{SS}(r)$ for oligomer P4b at T* = 1.5, 1.75, 2.0 and 2.25. d) $g_{SS}(r)$ for oligomers P4d at T* = 1.5, 1.75 and 2.0. e) $g_{SS}(r)$ for oligomer P4a at T* = 1.5, 1.75, and 2.0. f) $g_{SS}(r)$ for oligomer P4c at T* = 1.5, 1.75 and 2.0. Oligomers with moderate side chain – side

chain attraction P3a, P4b, and P4a (left column) show increased side chain – side chain aggregation as temperature decreases, while oligomers with weak side chain – side chain attraction P3c, P4d, and P4c (right column) show little side chain – side chain aggregation and no change in side chain – side chain aggregation with temperature. These trends are consistent with those of P3b and P3d shown in the main manuscript and indicate that side chain – side chain attraction is a key driving force for the transition from cylinders at high temperature to lamellar morphologies at low temperature for oligomers with side chains in the *–syn* orientation.